Nanoscale

Accepted Manuscript

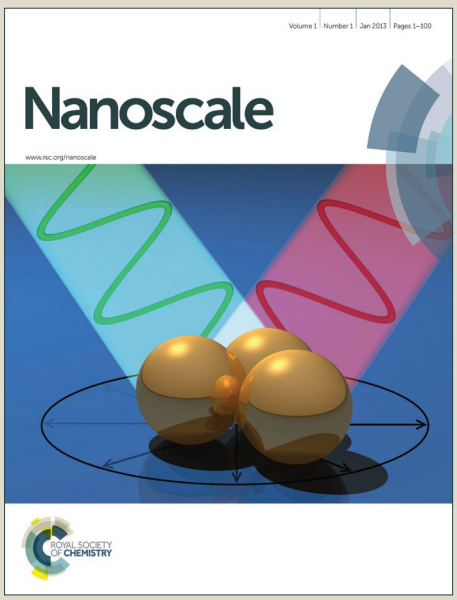

ROYAL SOCIETY OF CHEMISTRY

www.rsc.org/nanoscale

Nanoscale

PAPER

Oxidation-resistant hybrid metal oxide/metal nanodots/silver nanowires for high performance flexible transparent heaters

Received 00th January 20xx,
Accepted 00th January 20xx

DOI: 10.1039/x0xx00000x

www.rsc.org/

A–Young Kim,‡[a,b] Min Kyu Kim,‡[a,c] Chairul Hudaya,[a,d,e] Ji Hun Park,[f] Dongjin Byun,[b] Jong-Choo Lim[c] and Joong Kee Lee*[a,d]

Despite its excellent optical, electrical, mechanical, and thermal performances, a silver nanowire (AgNW)-based transparent conducting heater (TCH) still demonstrates several drawbacks such as facile nanowire breakdown on application of a high DC voltage, easy oxidation when exposed to harsh environments, leading to increased surface resistivity, and high resistance among wire junctions causing nonhomogeneous temperature profiles. To overcome these issues, the AgNW was hybridized with other transparent heating materials made of fluorine-doped tin oxide (FTO) thin film and NiCr nanodots (FTO/NiCr/AgNW). The dispersed NiCr nanodots (~ 50 nm) and FTO thin films (~ 20 nm) electrically bridge the nanowire junctions leading to a decreased sheet resistance and uniform temperature profiles. The hybrid transparent heater shows excellent optical transmittance (> 90%) and high saturation temperature (162 °C) at low applied DC voltage (6 V). Moreover, the FTO/NiCr/AgNW heater exhibits a stable sheet resistance in a hostile environment, hence highlighting the excellent oxidation-resistance of the heating materials. These results indicate that the proposed hybrid transparent heaters could be a promising approach to combat the inherent problems associated with AgNW-based transparent heaters for various functional applications.

Introduction

Flexible transparent conductive heaters (f-TCHs) have attracted enormous attention owing to their applicability to a broad range of devices, including wearable devices, outdoor displays, military equipment, sensors, vehicle windows, and heating systems as the defroster or defogger.[1-3] To date, tin-doped indium oxide (ITO) has been the most common choice as heating element because of its excellent optical transmittance and electrical conductivity.[4] However, ITO is not suitable for flexible designs and large scale applications because of its brittleness, slow thermal response, and indium scarcity, which leads to high cost.[5-7] As alternative materials to ITO, several transparent and conductive materials such as fluorine-doped tin oxide (FTO),[8] metal grids,[9] carbon nanotubes (CNTs),[10-13] graphene,[14, 15] and silver nanowires (AgNWs) have been used as f-TCHs. AgNW is one of the most promising candidates as an f-TCH material because of its flexibility, high transparency, excellent electrical conductivity, and easy fabrication.[16,17] Moreover, an AgNW-based heater presents a fast and high thermal response even at a low applied voltage.[18,19] Notwithstanding its excellent thermal performance, AgNW-based TCHs have some inherent drawbacks, including (1) high electrical resistance between the wire junctions leading to poor thermal uniformity,[20] (2) nanowire interconnection breakdown at a relatively high applied voltage, leading to discontinuous heating,[17] and (3) ease of oxidation when exposed to harsh environments such as increased temperature, humidity, or acidity. The last issue is particularly critical because TCHs are expected to endure such hostile conditions.

To overcome these problems, hybrid structures of AgNWs with other materials have been proposed, including a combination of the AgNW heater with 2-dimensional conductive films and various 1-dimensional materials such as metal grids, nanowires, and CNTs to obtain high optical transmittance and low surface resistivity, which in turn facilitates the generation of high temperatures when they are applied in TCHs.[21-26] Zhang et al. reported a reduced graphene oxide/AgNW heater with an optical transmittance (T) of 80% and a sheet resistance (R_s) of 27 Ω sq^{-1}.[21] Cheong et al. reported an ITO/AgNW heater with T = 85.1% and R_s = 50.9 Ω sq^{-1}.[23] Kang et al. reported an Ag-grid/graphene hybrid heater with T = 78% and R_s = 4 Ω sq^{-1}.[25] Huang et al. demonstrated a

[a] Center for Energy Convergence Research, Korea Institute of science and Technology (KIST), Hwarang-ro 14-gil 5, Seongbuk-gu, Seoul 136-791, Republic of Korea. E-mail: leejk@kist.re.kr
[b] Department of Material Science and Engineering, Korea University, Anam dong 5 ga, Seongbuk-gu, Seoul 136-701, Republic of Korea
[c] Department of Chemical and Biochemical Engineering, Dongguk University, Phil dong 3-26, Joong-gu, Seoul 100-715, Republic of Korea
[d] Department of Energy and Environmental Engineering, Korea University of Science and Technology, Gajungro 176, Yuseong-gu, Daejeon 305-350, Republic of Korea
[e] Department of Electrical Engineering, University of Indonesia, Kampus Baru UI, Depok, 16424, Indonesia
[f] Display team, Display group, IM Co., Ltd., 38 Madogongdan-ro 4-gil, Madomyeon, Hwaseong-si, Gyeonggi-do 445-861, Republic of Korea

† Electronic Supplementary Information (ESI) available: See DOI: 10.1039/x0xx00000x

‡ These authors contributed equally to this work.

method for embedding AgNWs into a polyimide film for designing a heater with T = 58.1% and R_s = 5.6 Ω sq^{-1}.[26]

However, these reported heaters do not fully satisfy the requirements for an ideal transparent heater, for which T must be high (> 90%) and R_s must be low (< 10 Ω sq^{-1}). However, it is natural that the increased T will be accompanied by increased R_s, because of the inclined film thickness.[16] In our previous study, scattered metal nanodots deposited on a glass substrate covered with an FTO thin film achieved high optical transmittance and uniformly distributed thermal profiles.[27] Most of all, it is very important that the high-performance TCH should provide low resistivity at high transmittance; at the same time, surface oxidation must be prevented for its use as a defroster. The surfaces of metal-based heaters get oxidized with time, which results in increased film resistance.

In this study, we fabricated a flexible hybrid transparent conductive heater (f-HTCH) using hybrid structure composed of an ultrathin FTO film, NiCr nanodots, and AgNWs, for producing high-transparency, low-surface-resistivity, and flexible conductive films. We find that the NiCr nanodots provide conductive pathways through the AgNWs. Furthermore, the FTO thin film prevents surface oxidation during cycling and provides a continuous conductive network between the AgNWs and the NiCr ultrathin film, thus improving the electrical properties of the hybrid conductive film. Therefore, the FTO/NiCr/AgNW f-HTCH exhibits high electrical and thermal performances such as improved temperature distribution, electrical conductivity, and optoelectronic property compared with metal-based heaters. Moreover, we characterized the mechanical flexibility of the f-HTCH during a bending test (10,000 cycles) for application to flexible devices, such as curved window surfaces or foldable electronic devices.

Results and discussion

Fig. 1a shows the schematic structure of the FTO/NiCr/AgNW f-HTCH. The diameters of the as-prepared NiCr/AgNW and FTO/NiCr/AgNW were ~30 and ~50 nm, respectively. The field-emission scanning electron microscopy (FE-SEM) images show the distribution of the AgNWs and the NiCr nanodots for NiCr/AgNW and FTO/NiCr/AgNW (Fig. 1b and c). To reveal the elemental composition of the f-HTCH, we performed scanning transmission electron microscopy (STEM) analysis (Fig. 1d), and corresponding energy-dispersive X-ray spectroscopy (EDX) measurements (Fig. 1e). Ni, Cr, Sn, O, and F are confirmed to be present in significant amounts, with peaks at energy levels of 0.84, 5.3, 3.6, 0.5, and 0.7 keV, respectively. We also observe strong peaks for Ag over the energy range of 2.6–3.4 keV. The Cu contributions to the spectrum are assumed to be due to the holey-carbon Cu grid support used during the EDX-STEM measurement.

A cross-sectional high-resolution transmission electron microscopy (HR-TEM) image of the FTO/NiCr/AgNW hybrid structure is shown in Fig. 2a.

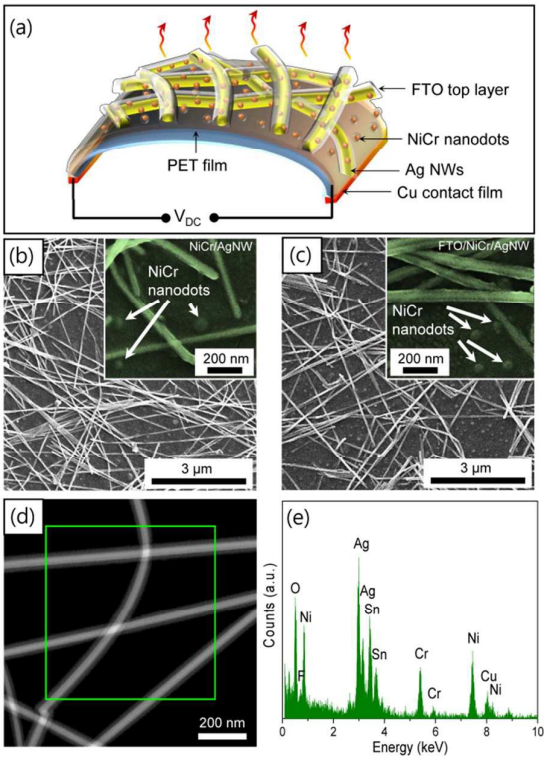

Fig. 1 (a) Schematic illustration of the FTO/NiCr/AgNW hybrid transparent heater. Top-view SEM images with low- and high-resolution (inset) for as-prepared (b) NiCr/AgNWs and (c) FTO/NiCr/AgNWs, respectively. (d) STEM image and (e) its corresponding EDX analysis of FTO/NiCr/AgNW transparent heater in the green square area of (d).

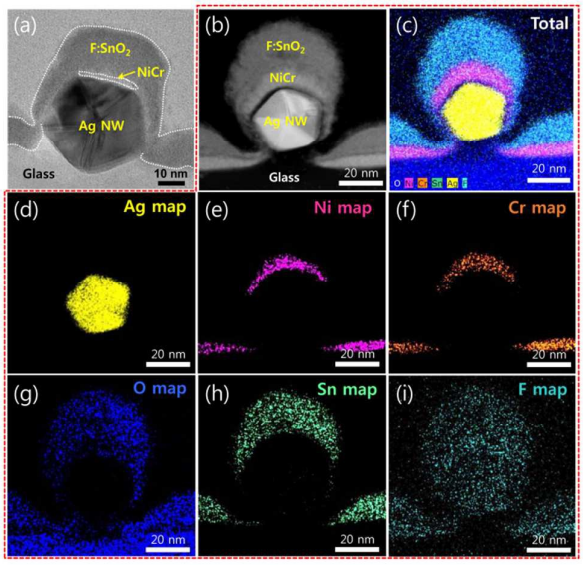

Fig. 2 (a) Cross-sectional TEM image of FTO/NiCr/AgNWs on glass after FIB cutting. (b) STEM image of FTO/NiCr/AgNWs and the corresponding TEM mapping images of the cross-sectioned FTO/NiCr/AgNWs show a clear distribution of (c) total, (d) Ag, (e) Ni, (f) Cr, (g) O, (h) Sn, and (i) F components.

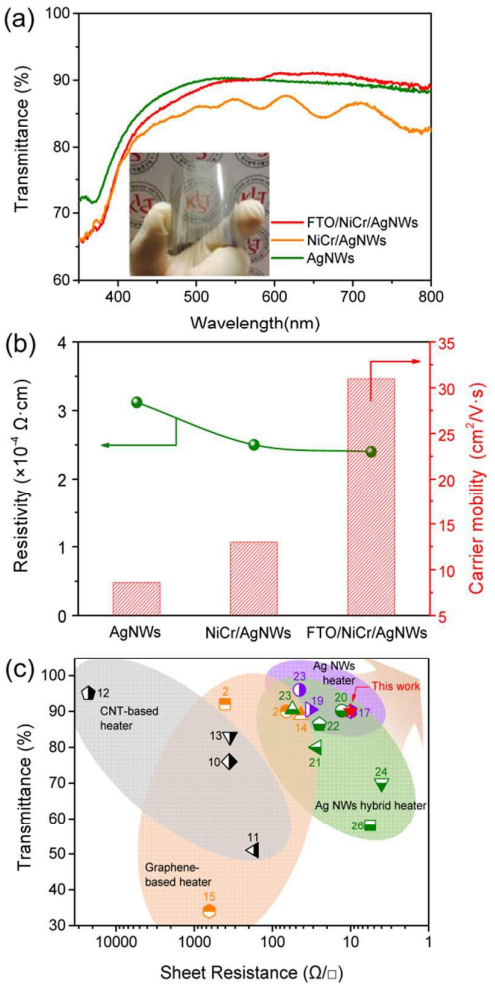

Fig. 3 (a) Visible optical transmittance spectra of the films in the wavelength range of 300–800 nm and a photograph of the FTO/NiCr/AgNW film is shown in the inset figure. (b) Carrier mobility and resistivity of the AgNWs, NiCr/AgNWs, and FTO/NiCr/AgNW hybrid transparent heaters obtained by Hall measurement (Note: The measurements were carried out directly to the as-prepared samples). (c) Plot of transmittance versus sheet resistance for FTO/NiCr/AgNWs and other heating systems from the literatures.

The cross-sectional STEM image with element mapping of the FTO/NiCr/AgNW also clearly reveals the distribution of the Ag, Ni, Cr, O, Sn, and F components (Fig. 2b-i). To optimize the performances of the transparent heaters, we have conducted a series of experiments on the AgNW, NiCr/AgNW, and FTO/NiCr/AgNW. As an initial assessment, the optical transmittances of the films were measured with different process parameters, as shown in Fig. S1†. We also measured the sheet resistance of the heaters by a four-point probe and estimated the Haacke's figure of merit ($\varphi_{TC} = T^{10}/R_s$) for the films,[28] where T is the transmittance at 550 nm and R_s is the average sheet resistance, as shown in Table S1†.

Fig. 3a shows the optical transmission spectra of the optimized AgNW, NiCr/AgNW, and FTO/NiCr/AgNW f-HTCHs in the wavelength range of 300–800 nm and a photograph of the flexible FTO/NiCr/AgNW heater in an inset. At 550 nm, the substrate-subtracted optical transmissions for AgNW, NiCr/AgNW, and FTO/NiCr/AgNW f-HTCHs are 89.92%, 86.98%, and 90.17%, respectively, which is favorable for transparent conductive materials. The lower transmittance of the NiCr/AgNW heater compared with that of the bare AgNWs can be attributed to the absorption and scattering of visible light by the rough ultrathin NiCr nanodots on the AgNW film. When an FTO thin film is coated on NiCr/AgNW, the optical transmittance is improved because the FTO thin film acts as an optical matching layer for reducing reflection of visible light from the metal surface, resulting in enhanced transparency in the visible wavelength range.[29] The electrical properties of the heaters were investigated using the Hall measurement system, as shown in Fig. 3b. The resistivities of the AgNW, NiCr/AgNW, and FTO/NiCr/AgNW heaters are 3.12, 2.5, and 2.4 × 10^{-4} Ω cm, respectively. The resistivity of the FTO/NiCr/AgNW heater drops significantly due to low sheet resistance caused by interconnection between AgNWs. The electrical resistivity of the heaters is closely related to the electron mobility of the heater materials.[30] The presence of NiCr-scattered nanodots and FTO thin films on the AgNW transparent heater has provided a fast pathway for electron transport inside the transparent heater, thereby exhibiting the highest carrier mobility and the lowest electrical resistivity value among other heater system. The transmittance versus sheet resistance plot (Fig. 3c) shows that the FTO/NiCr/AgNW f-HTCH has relative high performance, which is comparable to that of other reported transparent heaters.

Next, we investigate the heating performance of the f-HTCHs at a relatively low applied DC voltage of 6 V under ambient conditions due to safety and energy efficiency concerns. Fig. 4a shows the time-dependent temperature profiles of the AgNW, NiCr/AgNW, and FTO/NiCr/AgNW f-HTCHs; the temperature responses of the heaters were recorded using an infrared camera. The graph shows that the surface temperature of the f-HTCHs increases until reaching the saturation point. Compared with the other two heater types, the FTO/NiCr/AgNW heater achieved the highest saturation temperature (162 °C); however, the response times of all the HTCHs were under 30 s. The FTO/NiCr/AgNW film contributed to the outstanding thermal performance of the heater due to its excellent electrical properties, such as lower sheet resistance (9.9 Ω sq^{-1}) and higher electrical conductivity (4.16 ×10^3 S cm^{-1}). The heating rates of AgNW, NiCr/AgNW, FTO/NiCr/AgNW heaters are 0.425, 0.6, and 1.35 °C $V^{-1}s^{-1}$, respectively. Compared to other type of transparent heaters, the FTO/NiCr/AgNW heater exhibits the highest heating rate, pronouncing the important role of hybrid structure of the heaters. The FTO/NiCr/AgNW heater also enhanced the thermal uniformity, as captured by the thermal imaging camera (Fig. 4b). To assess the level of temperature uniformity, we applied equation, as below:[27]

$$T_{uniformity} = [(T_{max} - T_{min})/2\ T_{ave}] \times 100\% \quad (1)$$

where $T_{uniformity}$ (%) is the temperature uniformity and T_{max}, T_{min}, and T_{ave} are the highest, lowest, and average temperatures (°C), respectively.

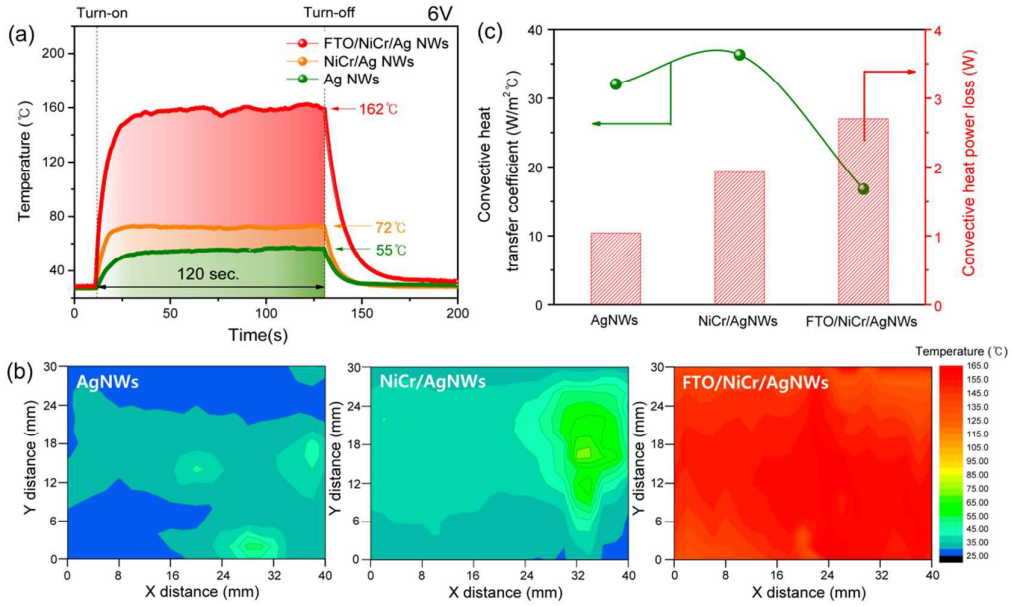

Fig. 4 (a) Time-dependent temperature profiles at an input voltage of 6 V and (b) the corresponding thermal conductivity and conductive heat-transfer coefficient of AgNWs, NiCr/AgNWs, and FTO/NiCr/AgNW hybrid transparent heaters (40 mm × 30 mm). (c) Contour maps for the saturation temperature of the heaters, which were captured after the 120 s heat test.

The maps suggest that the FTO/NiCr/AgNW heater shows the most uniform temperature ($T_{uniformity}$ = 13.80%), followed by bare AgNWs (62.0%) and NiCr/AgNW (46.63%). Its corresponding infrared images are shown in Fig. S2†. The temperature achieved by a heating system is generally a balance between the input power voltage and the heat loss.[2] Fig. 4c shows the convective heat-transfer coefficients and the convective heat power losses of the AgNW, NiCr/AgNW, and FTO/NiCr/AgNWs f-HTCHs. Convective heat power loss is expressed by equation,[31]

$$Q_c = h\,A\,(T_{sat} - T_s) \quad (2)$$

where h is the convective heat-transfer coefficient (W cm^{-2} °C^{-1}), A is the surface area (cm^2), T_{sat} is the saturation temperature (°C), and T_s is the initial surface temperature (°C). Furthermore, to investigate the power consumption of the hybrid heaters, the conductive heat-transfer coefficient was also calculated. Since the change in saturation temperature, depends on the input power, the convective heat-transfer coefficient can be obtained according to the equation,[2]

$$\Delta T_{sat} = V\,I\,/\,(h\,A) \quad (3)$$

where V is the applied voltage (V), and I is the current (A).[15] In general, convective heat transfer is directly influenced by the thermal solid–gas interfacial conductance. According to the degree of oxidation, the h value of material can change due to the different adsorption energies of the ambient gases. The oxidized surface will be trapped for a long enough period to absorb heat from the solid surface before releasing it. The thermal interfacial conductance is large in this case;[2] thus, the convective heat-transfer coefficient of the FTO/NiCr/AgNW heater (16.79 W cm^{-2} °C^{-1}) is smaller than that of the AgNW (32.05 W cm^{-2} °C^{-1}) and NiCr/AgNW heaters (36.32 W cm^{-2} °C^{-1}), which was expected based on the lower power consumption of the FTO/NiCr/AgNW heater.

To confirm surface oxidation, we performed the oxidation test by measuring the sheet resistance of the materials daily for 30 days in a room with saturated relative humidity. Fig. 5a shows the results of the oxidation test of the AgNW, NiCr/AgNW, and FTO/NiCr/AgNW f-HTCHs.

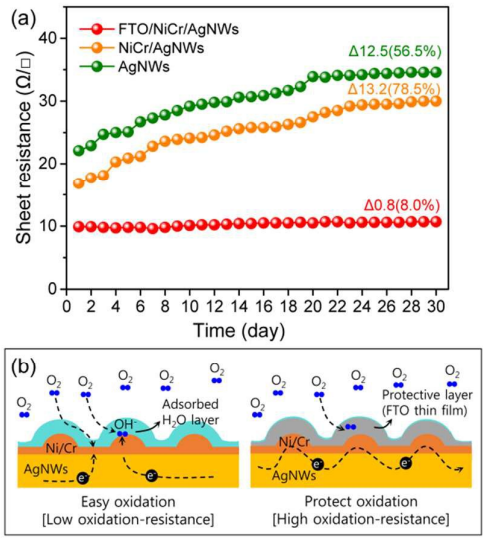

Fig. 5 (a) Results of the oxidation test with varying resistance for 30 days for the AgNWs, NiCr/AgNWs, and FTO/NiCr/AgNW hybrid transparent heaters. (b) Schematic illustration of the electron pathway in the heaters with and without a protective oxide layer.

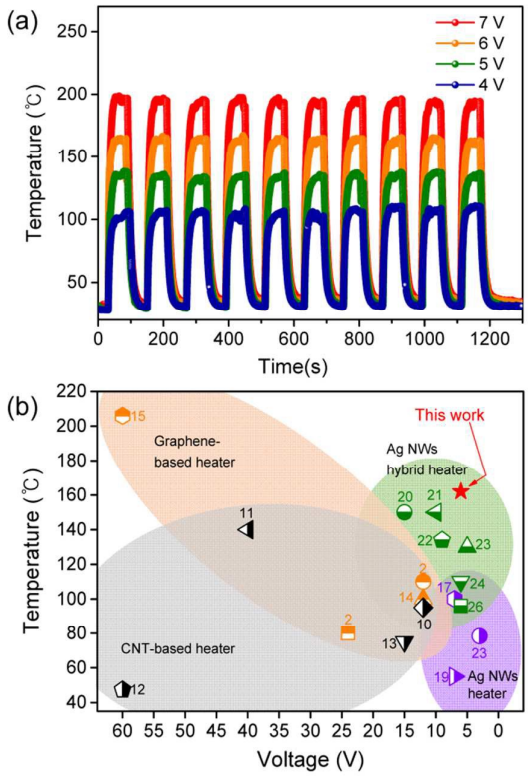

Fig. 6 (a) Fast heating and cooling tests of FTO/NiCr/AgNW hybrid transparent heaters under different input voltages. The voltage on/off interval was 60 s/60 s. (b) Saturation temperature of conductive transparent heaters, including those from the literatures.

The sheet resistances of the AgNW and the NiCr/AgNW films increased consistently over 30 days due to surface oxidation; however, the sheet resistance of the FTO/NiCr/AgNW film remained almost constant at 10 Ω sq^{-1}. The variations in sheet resistance for the AgNW, NiCr/AgNW, and FTO/NiCr/AgNW f-HTCHs were 12.5 (56.5%), 13.2 (78.5%), and 0.8 (8.0%), respectively. To explain the experimental observations, we hypothesize that cathodic protection occurs because of galvanic coupling, and a water layer can be adsorbed from the humid air, as schematized in Fig. 5b.[32] The outer FTO layer was used as a protective layer to cap the NiCr/AgNW film, preventing mechanical detachment of the nanomaterials and the oxidation of the NiCr/AgNW film. The coating layer thickness was controlled by adjusting its deposition time to obtain high transmittance (Fig. S1c†). The operational stability and temperature recoverability of the FTO/NiCr/AgNW f-HTCH are also investigated by performing life-time tests and subjecting the heater to repeated heat cycles under different applied voltages.

Fig. 6a shows the temperature responses of the heaters over 10 cycles under a voltage on/off interval of 60 s. The steady-state temperatures of the heaters at an applied voltage of 4, 5, 6, and 7 V are 110, 136, 162, and 193 °C, respectively, after the 10^{th} cycle.

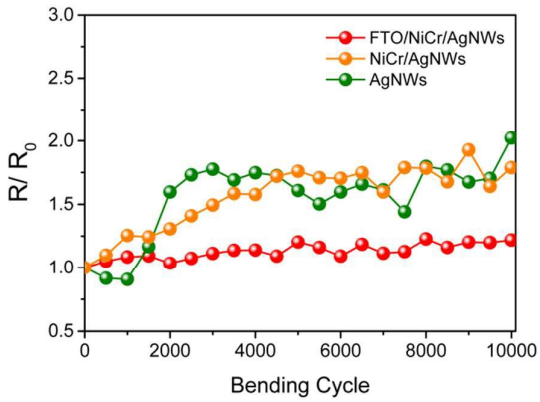

Fig. 7 Variations in the resistance of AgNWs, NiCr/AgNWs, and FTO/NiCr/AgNW hybrid transparent heaters during 10,000 cycles of bending tests.

The recovery between the highest and the lowest temperatures during the repeated heating and cooling tests was fast; this aspect is particularly important for applications requiring a fast thermal response. Fig. 6b compares our FTO/NiCr/AgNW f-HTCH with previously studied transparent heaters, such as CNT-, graphene-, AgNW-based ones.

To demonstrate the mechanical flexibility and durability of the fabricated f-HTCH when applied to the curved glasses of vehicles, we investigated the resistance variation of the heaters during a bending test (10,000 cycles), as shown in Fig. 7. The bending rate was one cycle per 1.748 s (0.572 Hz) and the resistance change of the heaters was observed for a bending strain of up to 0.68% ($\varepsilon = (d_s + d_f) / (2 \times R_c)$), where d_s and d_f are the average thicknesses of the substrate and the film, respectively, and R_c is the bending radius.[33] The resistances variation of the bare AgNW and NiCr/AgNW heaters increased to 102.23 and 162.62%, respectively, after 10,000 bending cycles. In contrast, it is important to note that only a small change (21.95%) can be observed in the resistance of the FTO/NiCr/AgNW f-HTCH after 10,000 bending cycles. These results indicated that the flexibility of the hybrid transparent heater improves and the binding between NiCr/AgNW becomes stronger by the addition of the FTO capping layer.

Experimental

Preparation of AgNWs-coated film.

We used a commercial AgNW dispersion (DT-AGNW-N30-1DI, Ditto Technology Co., Ltd.). The AgNWs were dispersed in deionized water at a concentration of 0.01mg mL^{-1}. The typical diameter and length of the AgNWs were 20–30 nm and 10–20 μm, respectively. The AgNW dispersion was coated on a polyethylene terephthalate (PET) film with a thickness of 110 μm using a blade, following which it was maintained in an oven at 80 °C for drying of the solvent. The coating thickness was controlled by adjusting the blade thickness.

Fabrication of NiCr nanodots

Scattered NiCr nanodots were deposited onto as-prepared AgNW films by a plasma-enhanced sputtering system. The base pressure was maintained below 10^{-5} Torr for 30 min and argon gas was supplied to the reactor at a constant flow rate of 25 sccm. To generate plasma, a radio frequency power of 80 W was applied to a NiCr (60:40%) target with a 4-inch diameter. The deposition time was 5 s and the substrate temperature was maintained at room temperature during the deposition process.

FTO-coated transparent heater

Deposition of an FTO thin layer as a protection layer onto an as-prepared NiCr/AgNWs/PET film was carried out using an electron cyclotron resonance-metal organic chemical vapor deposition system. The base pressure was maintained below 10^{-5} Torr. Tetramethyltin (TMT) as a precursor for tin, sulfur hexafluoride as a fluorine doping agent, hydrogen, and oxygen gases were introduced to the chamber, and their flow rates were kept constant at 6, 0.75, 4.5, and 40 sccm, respectively. The metal organic source canister in the chiller was maintained at a constant temperature of −10.2 °C, and argon gas was used as a carrier gas for TMT. The bubbler and working pressures were 43.6 Torr and 10 mTorr, respectively. Deposition was performed at a constant microwave power of 1400 W, a frequency of 2.45 GHz, and a magnetic current of 160 A for 20 s at room temperature.

AgNWs-based hybrid transparent heaters

For temperature measurements, hybrid transparent heaters were manufactured by cutting the samples into 50 mm × 30 mm pieces. Copper tapes (5 mm × 30 mm) were attached to each edge of the heater. A DC voltage was applied (PTDT-101HR-BI, Power TM) to measure current at a given input voltage. The temperature of the film was measured in real time at room temperature by an infrared (IR) thermometer (E-30, FLIR). For the oxidation test, the AgNW, NiCr/AgNW, and FTO/NiCr/AgNW films were put in a room with saturated relative humidity for 30 days, and we measured the sheet resistance every day.

Characterization

The morphology of the heaters was observed by FE-SEM (Hitachi S-4100) at an accelerated voltage of 15 kV. To further confirm the thicknesses of metal nanodots and FTO thin layer, the heaters were prepared by focused ion beam (FIB, Nova FIB) to analyze the TEM (Titan) with EDX and mapping operated at 200 kV. The electrical and optical properties of the heaters were determined using Hall effect measurements (HMS-3000, Ecopia) and ultraviolet-visible spectroscopy (UV−Vis, Varian 5000), with a PET film used as the reference. The sheet resistance of the heaters was measured using a four-point probe equipment (Mitsubishi Chemical Analytech, MCP-T610). The bending test was carried out with a lab-made apparatus (IM Co., Ltd.) equipped with software for recording the film resistance and cycle number.

Conclusions

We report a hybrid flexible AgNW transparent heater composed of an FTO thin film and scattered NiCr nanodots. Heating materials deposited on a PET substrate show remarkable performances, including excellent optical transmittance, fast and high thermal response, high oxidation-resistance, and robust endurance against repeated bending cycles. The presence of both NiCr nanodots and FTO thin films on the surface of the AgNW heater are evidenced to decrease the surface resistivity and increase the thermal uniformity of the heater as they conductively interconnect the nanowire junctions. As a result, our hybrid heater outperforms other hybrid-type AgNW f-HTCH, including carbonaceous, polymer and metal-based heating materials, hence making it a suitable heating material for home and any industrial appliances.

Acknowledgements

This work was supported by KIST institutional program (Project No. 2E25304) and Nano-Convergence Foundation (www.nanotech2020.org) funded by the Ministry of Science, ICT and Future Planning (MSIP, Korea) & the Ministry of Trade, Industry and Energy (MOTIE, Korea) [Project Name: Development of Functional Smart Film Manufacturing Technologies].

Notes and references

1 D. S. Hecht, L. B. Hu and G. Irvin, *Adv. Mater.*, 2011, **23**, 1482-1513.
2 J. J. Bae, S. C. Lim, G. H. Han, Y. W. Jo, D. L. Doung, E. S. Kim, S. J. Chae, T. Q. Huy, N. V. Luan and Y. H. Lee, *Adv. Funct. Mater.*, 2012, **22**, 4819-4826.
3 S. Sorel, D. Bellet and J. N. Coleman, *Acs Nano*, 2014, **8**, 4805-4814.
4 S. J. Hong, S. W. Kim and J. I. Han, *Jpn. J. Appl. Phys.*, 2014, **53**, 08NF04.
5 A. Kumar and C. W. Zhou, *Acs Nano*, 2010, **4**, 11-14.
6 P. C. Hsu, S. Wang, H. Wu, V. K. Narasimhan, D. S. Kong, H. R. Lee and Y. Cui, *Nat. Commun.*, 2013, **4**, 2522.
7 B. Han, K. Pei, Y. L. Huang, X. J. Zhang, Q. K. Rong, Q. G. Lin, Y. F. Guo, T. Y. Sun, C. F. Guo, D. Carnahan, M. Giersig, Y. Wang, J. W. Gao, Z. F. Ren and K. Kempa, *Adv. Mater.*, 2014, **26**, 873-877.
8 A. Y. Kim, K. Lee, J. H. Park, D. Byun and J. K. Lee, *Phys. Status Solidi A*, 2014, **211**, 1923-1927.
9 Y. Jang, J. Kim and D. Byun, *J. Phys. D: Appl. Phys.*, 2013, **46**, 155103.
10 Y. H. Yoon, J. W. Song, D. Kim, J. Kim, J. K. Park, S. K. Oh and C. S. Han, *Adv. Mater.*, 2007, **19**, 4284-4287.
11 D. Jung, D. Kim, K. H. Lee, L. J. Overzet and G. S. Lee, *Sens. Actuators A*, 2013, **199**, 176-180.
12 T. J. Kang, T. Kim, S. M. Seo, Y. J. Park and Y. H. Kim, *Carbon*, 2011, **49**, 1087-1093.
13 H. S. Jang, S. K. Jeon and S. H. Nahm, *Carbon*, 2011, **49**, 111-116.
14 J. Kang, H. Kim, K. S. Kim, S. K. Lee, S. Bae, J. H. Ahn, Y. J. Kim, J. B. Choi and B. H. Hong, *Nano Lett.*, 2011, **11**, 5154-5158.
15 D. Sui, Y. Huang, L. Huang, J. J. Liang, Y. F. Ma and Y. S. Chen, *Small*, 2011, **7**, 3186-3192.

16 L. B. Hu, H. S. Kim, J. Y. Lee, P. Peumans and Y. Cui, *Acs Nano*, 2010, **4**, 2955-2963.
17 T. Y. Kim, Y. W. Kim, H. S. Lee, H. Kim, W. S. Yang and K. S. Suh, *Adv. Funct. Mater.*, 2013, **23**, 1250-1255.
18 I. K. Moon, J. I. Kim, H. Lee, K. Hur, W. C. Kim and H. Lee, *Sci. Rep.*, 2013, **3**, 1112.
19 C. Celle, C. Mayousse, E. Moreau, H. Basti, A. Carella and J. P. Simonato, *Nano Res.*, 2012, **5**, 427-433.
20 J. S. Woo, J. T. Han, S. Jung, J. I. Jang, H. Y. Kim, H. J. Jeong, S. Y. Jeong, K. J. Baeg and G. W. Lee, *Sci. Rep.*, 2014, **4**, 4804.
21 X. Zhang, X. B. Yan, J. T. Chen and J. P. Zhao, *Carbon*, 2014, **69**, 437-443.
22 J. Li, J. Liang, X. Jian, W. Hu, J. Li and Q. Pei, *Macromol. Mater. Eng.*, 2014, **299**, 1403-1409.
23 H.-G. Cheong, D.-W. Song and J.-W. Park, *Microelectron. Eng.*, 2015, **146**, 11-18.
24 S. L. Ji, W. W. He, K. Wang, Y. X. Ran and C. H. Ye, *Small*, 2014, **10**, 4951-4960.
25 J. Kang, Y. Jang, Y. Kim, S. H. Cho, J. Suhr, B. H. Hong, J. B. Choi and D. Byun, *Nanoscale*, 2015, **7**, 6567-6573.
26 Q. Huang, W. Shen, X. Fang, G. Chen, J. Guo, W. Xu, R. Tan and W. Song, *RSC Adv.*, 2015, **5**, 45836-45842.
27 C. Hudaya, B. J. Jeon and J. K. Lee, *Acs Appl. Mater. Interfaces*, 2015, **7**, 57-61.
28 G. Haacke, *J. Appl. Phys.*, 1976, **47**, 4086-4089.
29 K. H. Kim and Q. H. Park, *Opt. Express*, 2014, **22**, 1964-1971.
30 A. Dhar and T. L. Alford, *ECS Solid State Lett.*, 2014, **3**, N33-N36.
31 Z. Q. Zhai and Q. Y. Chen, *Build. Environ.*, 2004, **39**, 1001-1009.
32 R. Sachan, V. Ramos, A. Malasi, S. Yadavali, B. Bartley, H. Garcia, G. Duscher and R. Kalyanaraman, *Adv. Mater.*, 2013, **25**, 2045-2050.
33 Z. Suo, E. Y. Ma, H. Gleskova and S. Wagner, *Appl. Phys. Lett.*, 1999, **74**, 1177-1179.